PHOTONIC SENSORS / Vol. 10, No. 1, 2020: 88–96

Impact Localization of CFRP Structure Based on FBG Sensor Network

Yaozhang SAI[1*], Xiuxia ZHAO[2], Lili WANG[1], and Dianli HOU[1]

[1]*School of Information and Electrical Engineering, Ludong University, Yantai 264025, China*

[2]*TIANRUN CRANKSHAFT CO., LTD, Wendeng 264400, China*

[*]Corresponding author: Yaozhang SAI E-mail: saiyaozhang@163.com

Abstract: Low energy impact can induce invisible damage of carbon fiber reinforced polymer (CFRP). The damage can seriously affect the safety of the CFRP structure. Therefore, damage detection is crucial to the CFRP structure. Impact location information is the premise of damage detection. Hence, impact localization is the primary issue. In this paper, an impact localization system, based on the fiber Bragg grating (FBG) sensor network, is proposed for impact detection and localization. For the completed impact signal, the FBG sensor and narrow-band laser demodulation technology are applied. Wavelet packet decomposition is introduced to extract available frequency band signals and attenuate noise. According to the energy of the available frequency band signal, an impact localization model, based on the extreme learning machine (ELM), is established with the faster training speed and less parameters. The above system is verified on the 500 mm × 500 mm × 2 mm CFRP plate. The maximum localization error and the minimum localization error are 30.4 mm and 6.7 mm, respectively. The average localization error is 14.7 mm, and training time is 0.7 s. Compared with the other machine learning methods, the localization system, proposed in this paper, has higher accuracy and faster training speed. This paper provides a practical system for impact localization of the CFRP structure.

Keywords: Carbon fiber reinforced polymer; fiber Bragg grating; extreme learning machine; impact localization; wavelet packet decomposition

Citation: Yaozhang SAI, Xiuxia ZHAO, Lili WANG, and Dianli HOU, "Impact Localization of CFRP Structure Based on FBG Sensor Network," *Photonic Sensors*, 2020, 10(1): 88–96.

1. Introduction

Carbon fiber reinforced polymer (CFRP) is a very important structural material of the aerospace vehicle. It has high strength, weight ratio, and strong resistance to corrosion [1, 2]. In the future, CFRP will play a more crucial role in the aerospace field. But when CFRP is impacted by the low energy impact load, the invisible damages can appear [3, 4]. If the damages are not detected in time, the safety of the CFRP structure will be threatened [5, 6]. Therefore, the accurate detection of impact is very essential.

The key of impact detection mainly includes impact signal acquisition and localization. The traditional sensors for impact detection are difficult to be widely used in the aerospace vehicle due to the weight and volume. Hence, there is an urgent need of the lighter and smaller sensor. Fiber Bragg grating (FBG) is the suitable sensor for impact detection of

Received: 15 November 2018 / Revised: 31 January 2019

DOI: 10.1007/s13320-019-0546-9
Article type: Regular

the aerospace vehicle. Shrestha *et al.* [7] used the FBG to acquire the impact signal, and Yu *et al.* [8] applied FBG sensors to detect the low frequency impact signal. Zhao *et al.* [9] used the FBG to acquire the strain wave for impact detection. According to the strain amplitude, impact localization can be realized. Despite the FBG has been utilized for impact detection, only the low frequency strain wave is acquired. It is insufficient to complete high accuracy impact localization. Therefore, the high-speed demodulation system is necessary for impact localization.

In recent years, many impact localization methods are studied. Fu *et al.* [10] applied the back propagation neural network (BPNN) for impact localization in the CFRP plate. Zhu *et al.* [11] used the parameterized laminate model to acquire the location of impact. Zhao *et al.* [12] utilized the hybrid minimization algorithm and integrated wavelet transform to calculate the impact location with high accuracy. Although the above methods have high localization accuracy, the wave velocity is necessary. However, wave velocity is anisotropic in the CFRP structure. Furthermore, wave velocities of different frequency signals are different. The acquisition of accurate wave velocity information is not easy. Hence, it is obvious that localization methods without requiring the wave velocity are necessary for the CFRP structure. Kundu *et al.* [13] used two triangular sensor arrays to locate the impact source in the composite material, and Ciampa *et al.* [14] applied a similar localization principle for the impact localization with six sensors. These methods do not require the wave velocity, but the localization accuracy is not high when impact sources are near to the sensor array. Shrestha *et al.* [15, 16] used the error outlier algorithm to locate impact in the composite structure and wing structure. At the same time, Kim *et al.* [17] applied Pugh's concept selection to improve the error outlier algorithm for the improvement of the impact localization. Alajlouni *et al.* [18] used the relationship between the energy-attenuation of waves and traveled distance to acquire the impact location. Although the above algorithms do not need the wave velocity, the localization accuracy is not high because of the sensor array character or localization algorithm. In recent years, machine learning is used for the impact localization. Lu *et al.* [19] applied least squares support vector machine (LS-SVM) to locate impact. The wave velocity is not necessary in the method. But the time difference sample, which is the key of the LS-SVM, is easily disturbed by noise. At the same time, the LS-SVM has many parameters and takes a long time to learn to use.

In this paper, FBG sensors and high-speed demodulation are applied to acquire impact signals on the CFRP plate. For the impact localization, wavelet packet decomposition is used to obtain different frequency band impact signals. The energy of the signal is calculated as the characteristic sample. For the high accuracy localization, an extreme learning machine (ELM), which needs only one parameter, is applied. According to the energy sample and ELM, a strong localization model can be obtained. Comparative experiments are carried on to verify the performance of localization algorithm.

2. Signal processing and localization algorithm

2.1 Wavelet packet decomposition

The impact signal is the broadband signal, and the energies of each frequency band signals are different. With the increasing propagation distance, the energy attenuation is different. Therefore, the distances between the impact source and sensors can be confirmed by the energy change of different frequency band signals. So, the energies of different frequency band signals are the key of the localization. In this paper, wavelet packet decomposition is introduced to extract different frequency band signals and calculate energies. The

available frequency band signals, whose energy attenuations are obvious, are used to locate impact by energy analysis. At the same time, noise and low energy signals are removed for high accuracy impact localization.

According to the wavelet packet decomposition, orthogonal scale function $\phi(t)$ and wavelet function $\varphi(t)$ can be expressed as

$$\begin{cases} \phi(t)=\sqrt{2}\sum_k h(k)\phi(2t-k) \\ \varphi(t)=\sqrt{2}\sum_k g(k)\varphi(2t-k) \end{cases} \tag{1}$$

where $h(k)$ and $g(k)$ are filter coefficients; k and t are translation quantity and independent variable, respectively. According to the multi resolution analysis and Mallat algorithm, wavelet packet decomposition and reconstruction can be expressed as

$$\begin{cases} d_{j+1,2n}(k)=\sum_l \bar{h}(2k-l)d_{j,n}(l) \\ d_{j+1,2n+1}(k)=\sum_l \bar{g}(2k-l)d_{j,n}(l) \\ d_{j,n}(k)=\sum_l h(k-2l)d_{j+1,2n}(l)+\sum_l g(k-2l)d_{j+1,2n+1}(l) \end{cases} \tag{2}$$

where $\bar{h}$ and $\bar{g}$ are the dual operators of h and g, respectively; j and n are the scale factor and decomposition level, respectively; $d_{j,n}(k)$ is the wavelet packet coefficient.

Given the signal is decomposed into i layers by wavelet packet decomposition, the wavelet packet scale is 2^i. According to the wavelet packet decomposition, the signal $s(t)$ can be represented as

$$s(t)=\sum_{y=1}^{2^i} s_{iy}(t) \tag{3}$$

where $s_{iy}(t)$ is the yth wavelet packet reconstruction signal in the ith layer. The energy of $s(t)$ can be rearranged as

$$E=\sum_{y=1}^{2^i} e_{iy} \tag{4}$$

where e_{iy} is the energy of the yth signal in the ith layer signal decomposition. At the same time, it can be defined as follows:

$$e_{iy}=\int_{-\infty}^{+\infty} s_{iy}^2(t)\mathrm{d}t\,. \tag{5}$$

According to i and y, the frequency range of each decomposition signal can be confirmed. Due to e_{iy}, the energy distribution can be acquired for impact signal analysis.

2.2 Extreme learning machine

ELM is a single hidden-layer feed-forward neural network learning method. In the ELM network, initial input weights and hidden layer biases are randomly assigned. ELM can be defined as

$$\mathbf{y}_i=\sum_{j=1}^{L}\beta_j g(\boldsymbol{\omega}_j\mathbf{x}_i+b_j) \tag{6}$$

where ($\mathbf{x}_i$, $\mathbf{t}_i$) is the set of N distinct samples; L is the node number of hidden layer; β_j is the output weights, and $g(\cdot)$ represents the activation function; $\boldsymbol{\omega}_j$ is the input weights, and b_j is the biases of the jth hidden layer. The learning aim of the ELM is the minimum output error as follows:

$$\sum_{i=1}^{N}\|\mathbf{y}_i-\mathbf{t}_i\|=0\,. \tag{7}$$

Therefore, (6) can be rearranged as follows:

$$\mathbf{t}_i=\sum_{j=1}^{L}\beta_j g(\boldsymbol{\omega}_j\mathbf{x}_i+b_j)\,. \tag{8}$$

Assuming $h_{ij}=g(\boldsymbol{\omega}_j\mathbf{x}_i+b_j)$ and $\mathbf{H}=(h_{ij})_{N\times L}$, (8) can be redefined as

$$\mathbf{T}=\mathbf{H}\boldsymbol{\beta} \tag{9}$$

where $\mathbf{T}=(\mathbf{t}_1,\mathbf{t}_2,\cdots,\mathbf{t}_N)$ and $\boldsymbol{\beta}=(\beta_1,\beta_2,\cdots,\beta_L)$. When $\boldsymbol{\omega}_j$ and b_j are randomly assigned, $\mathbf{H}$ can be uniquely confirmed. The training process of the ELM can be equivalent to obtain the least squares solution as follows:

$$\|\mathbf{H}\bar{\boldsymbol{\beta}}-\mathbf{T}\|=\min_{\boldsymbol{\beta}}\|\mathbf{H}\boldsymbol{\beta}-\mathbf{T}\|\,. \tag{10}$$

According to Moore-Penrose generalized inverse, the result can be expressed as

$$\bar{\boldsymbol{\beta}}=\bar{\mathbf{H}}\mathbf{T} \tag{11}$$

where $\bar{\mathbf{H}}$ the is Moore-Penrose generalized inverse matrix of $\mathbf{H}$ [20]. The ELM structure is

shown in Fig. 1.

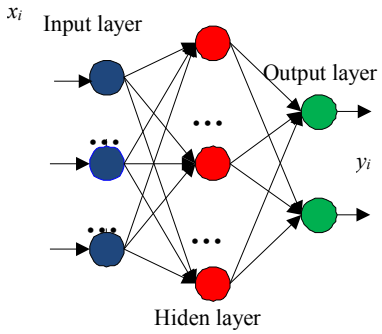

Fig. 1 ELM structure.

2.3 Localization process

The impact localization algorithm based on the wavelet packet decomposition and ELM is as follows:

(1) According to the monitoring areas, samples are obtained by impact experiments, including the impact signal and coordinate information.

(2) According to the wavelet packet decomposition, the different frequency band signals are obtained, and energies are calculated. For high accuracy localization, the energies of the frequency band signals, whose attenuations are obvious with increasing the propagation distance, are extracted for the input of the ELM model.

(3) By using the normalized energy and impact coordinate form training samples, the ELM model is trained for impact localization. When impact appears, the energy information of the impact signal is normalized and input to the ELM model. The model will output the accurate coordinate of impact.

3. Impact localization

3.1 Experimental setup

In this paper, FBG sensors are applied to obtain impact signals. Because the impact signal is a wide band signal, for acquiring the completed impact signal, a high-speed FBG demodulation system is necessary. In this paper, the narrow-band laser demodulation technology is used for impact signals. The demodulation system is shown in Fig. 2, which includes the narrow-band laser, coupler, circulator, FBG, photoelectric converter, amplifier, and data acquisition system. The reflectance wavelengths of four FBG sensors are 1565.255 nm, 1565.250 nm, 1565.255 nm, and 1565.260 nm, respectively. The grating length of the FBG is 10 mm. For narrow-band laser demodulation, the central wavelength of narrow-band laser is set as 1565.280 nm, and the output power is 10 mW. Narrow-band laser is Santec TSL-510, and the bandwidth of the spectrum is less than 0.1 pm. The sample frequency of the data acquisition system is 5 MHz. The system has a high-pass filter, whose frequency is 1 kHz.

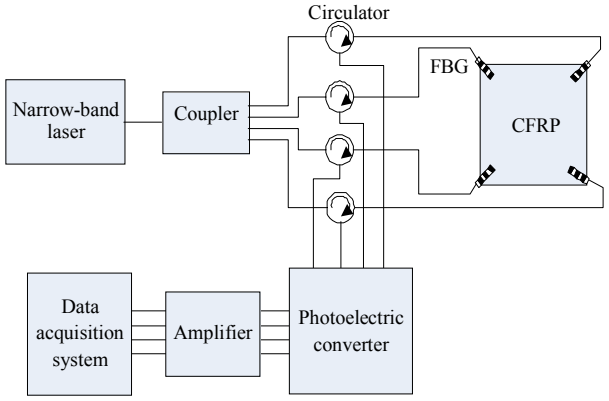

Fig. 2 FBG demodulation system.

There is a 500 mm × 500 mm × 2 mm CFRP plate. The monitor area of CFRP is 300 mm × 300 mm, as shown in Fig. 3. Four FBG sensors are pasted in four corners of the monitoring area by epoxy glue, and the coordinates are (0, 300), (300, 300), (300, 0), and (0, 0). The angle between the axial direction of FBG and the boundary of monitoring area is 45 degree. The monitor area is divided into 30 small areas. Impact is simulated by steel ball impact, and the impact energy is 0.2 J.

3.2 Impact localization

The line between FBG1 and FBG3 is obtained to study the relationship between the impact signals energy characteristics and distance. In the line, seven points are selected for impact. The distances

between these points and FBG3 are 70 mm, 140 mm, 210 mm, 280 mm, 350 mm, and 420 mm, respectively. The impact signals are shown in Fig. 4. The signals indicate that the amplitude of the signal significantly decreases with increasing distance between the impact source and FBG3. The frequency spectrum of the impact signal is shown in Fig. 5, and the frequency range is 1 kHz – 40 kHz. Therefore, the signal components are complex. At the same time, due to the system noise, the accurate relationship between the amplitude and distance is not easy to be established.

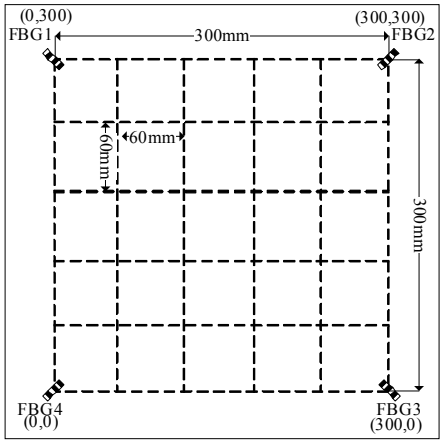

Fig. 3 Experiment layout of CFRP.

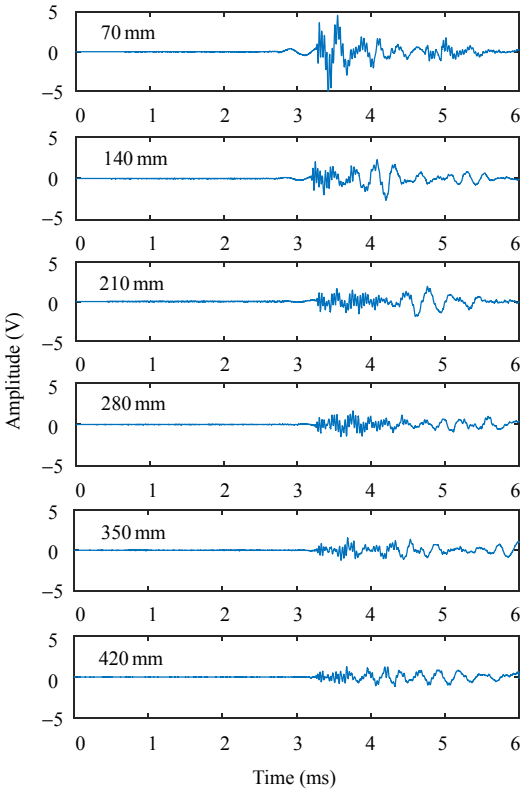

Fig. 4 Impact signals.

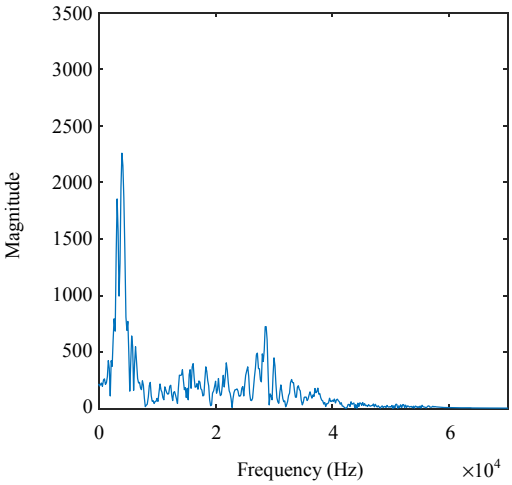

Fig. 5 Frequency spectrum of impact signal.

In this paper, we introduce the wavelet packet decomposition to analyze the impact signal and look for the connection between the signal characteristics and distance. The wavelet packet function is sym4. The layer number of wavelet packet decomposition is 6, and 64 different frequency band signals are obtained. The frequency band range can be calculated by $(n-1)f/2^{(i+1)} - nf/2^{(i+1)}$, $n = 1, 2, \cdots, 64$, i is the layer number, and f is the sample frequency. So, the frequency bandwidth of the decomposition signal approximately is 3.9 kHz. Because the frequency range of impact is 1 kHz – 40 kHz, the decomposition signals in the frequency range are extracted, as shown in Fig. 6. According to the decomposition signals, the amplitudes of S1, S2, S3, and S4 are more than 0.05 V. Therefore, the

energy of the impact signal mainly focuses on the four frequency bands which are 0 kHz – 3.9 kHz, 3.9 kHz – 7.8 kHz, 7.8 kHz – 11.7 kHz, and 11.7 kHz – 15.6 kHz, respectively. We calculate the energies of the four frequency band signals, as shown in Fig. 7. The energies significantly reduce with increasing distance between the impact point and FBG3. According to five-order polynomial fitting, the relationship between the energy and distance can be accurately obtained. According to the signals of multiple sensors at different locations, the impact localization can be implemented. Because the energies of the frequency band 7.8 kHz – 11.7 kHz and 11.7 kHz – 15.6 kHz are small, the energies of 0 kHz – 3.9 kHz and 3.9 kHz – 7.8 kHz are used for the impact localization.

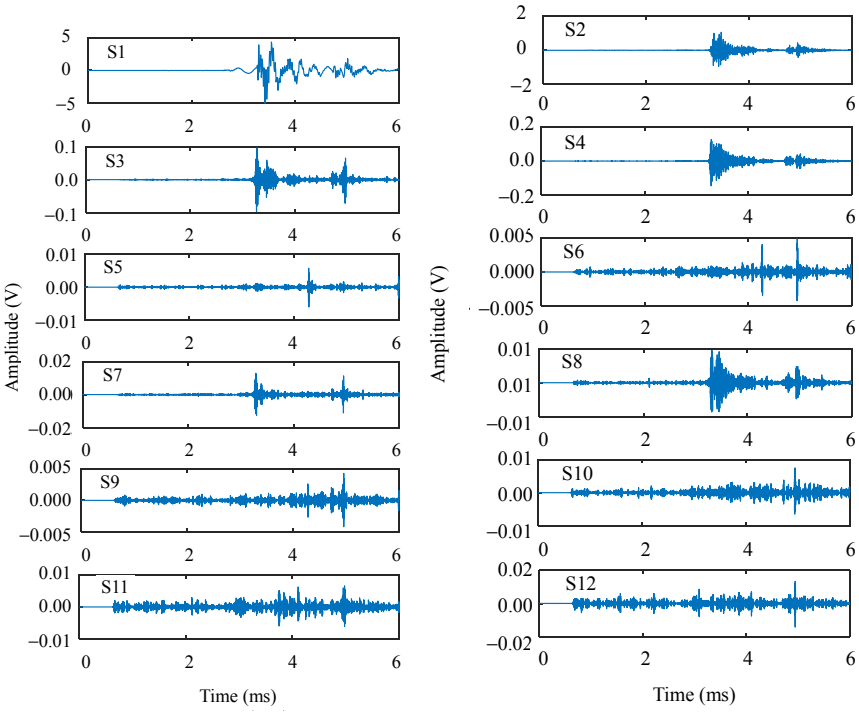

Fig. 6 Decomposition signals.

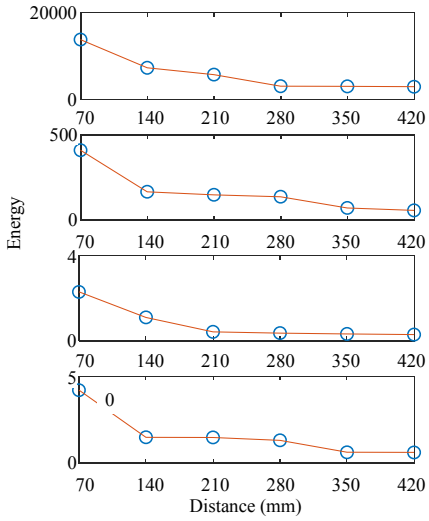

Fig. 7 Relationship between the energies and distance.

In this paper, ELM is applied to obtain the accurate relationship model between the signal energy and impact location. According to the monitored area of the CFRP plate, ten points are selected for impact experiments in each small area of the monitored area. 250 groups of signals are obtained. According to the wavelet packet decomposition, the signal energies of 0 kHz – 3.9 kHz and 3.9 kHz – 7.8 kHz are calculated and normalized. According to the normalized energy eigenvector and the impact coordinates, the training sample set is established, and ELM is trained for the impact localization. The node number of the ELM hidden layer is 10.

For verifying the ELM model, the impact

experiment is implemented at (190 mm, 250 mm). The signals are shown in Fig. 8. According to the wavelet packet decomposition, the energies of the designated frequency band signals are calculated, as shown in Fig. 9. The normalized energies of four FBG sensors are input to the impact localization model based on the ELM. The coordinate is output, and it is (197 mm, 256 mm). The radial error is 9.2 mm. In order to verify the reliability and accuracy of the ELM model, 15 impact points are randomly selected for experiments with different algorithms. The localization results and errors are shown in Figs. 10 and 11, and Table 1. From the results, the maximum localization errors of the ELM, support vector regression (SVR) and back-propagation (BP) neural network, are 30.4 mm, 40.0 mm, and 38.1 mm, respectively. The minimum localization errors of three algorithms are 6.7 mm, 8.9 mm, and 9.8 mm, respectively. The average errors are 14.2 mm, 20 mm, and 23.1 mm, respectively. It is obvious that the ELM algorithm has higher localization accuracy. In addition, the training time is an important index for the ELM, SVR, and BP neural network. In localization experiments, the training time of the above algorithms are 0.7 s, 1.6 s, and 3.2 s, respectively. Compared with the SVR and BP neural network, the ELM has higher localization and less training time consumption. Furthermore, only the node number of the hidden layer needs to be adjusted. The results are calculated by MATLAB 7.1 and computer with AMD A8-5600K 3.6 GHz CPU.

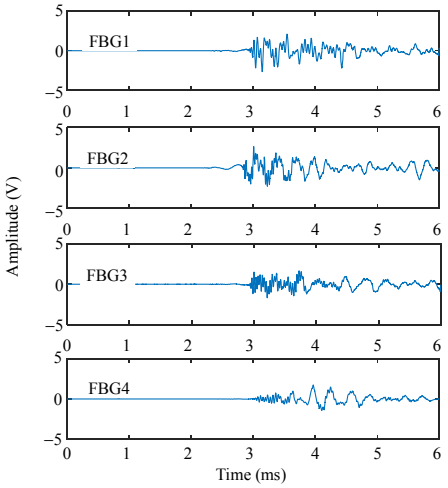

Fig. 8 Localization signals.

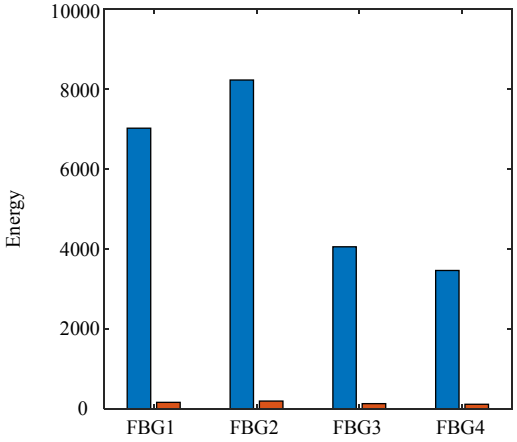

Fig. 9 Energies of decomposition signals.

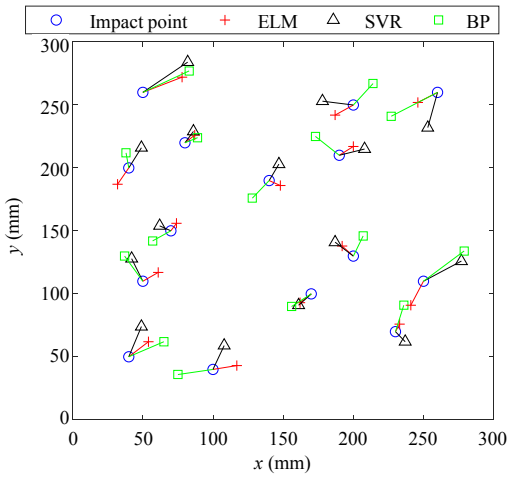

Fig. 10 Impact localization results.

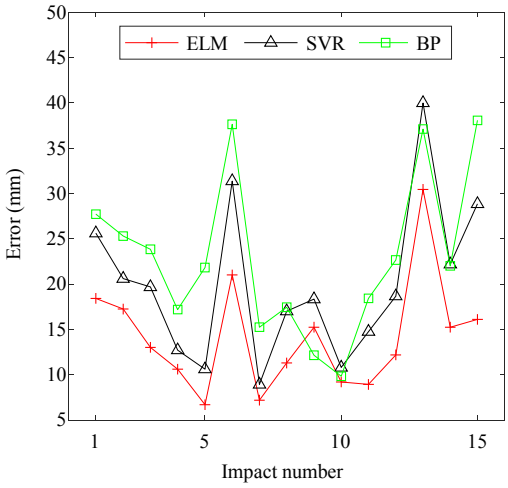

Fig. 11 Impact localization errors.

Table 1 Impact localization result.

Impact number	Impact coordinate (mm)	ELM algorithm (mm)	ELM error (mm)	SVR algorithm (mm)	SVR error (mm)	BP algorithm (mm)	BP error (mm)
1	(40, 50)	(54, 62)	18.4	(49, 74)	25.6	(65, 62)	27.7
2	(100, 40)	(117, 43)	17.3	(108, 59)	20.6	(75, 36)	25.3
3	(50, 110)	(61, 117)	13.0	(42, 128)	19.7	(37, 130)	23.9
4	(170, 100)	(162, 93)	10.6	(161, 91)	12.7	(156, 90)	17.2
5	(230, 70)	(233, 76)	6.7	(237, 62)	10.6	(236, 91)	21.8
6	(250, 110)	(241, 91)	21.0	(277, 126)	31.4	(279, 134)	37.6
7	(70, 150)	(74, 156)	7.2	(62, 154)	8.9	(57, 142)	15.3
8	(200, 130)	(192, 138)	11.3	(187, 141)	17.0	(207, 146)	17.5
9	(40, 200)	(32, 187)	15.3	(49, 216)	18.4	(38, 212)	12.2
10	(80, 220)	(87, 226)	9.2	(86, 229)	10.8	(89, 224)	9.8
11	(140, 190)	(148, 186)	8.9	(147, 203)	14.8	(128, 176)	18.4
12	(190, 210)	(200, 217)	12.2	(208, 215)	18.7	(173, 225)	22.7
13	(50, 260)	(78, 272)	30.4	(82, 284)	40.0	(83, 277)	37.1
14	(200, 250)	(187, 242)	15.3	(178, 253)	22.2	(214, 267)	22.0
15	(260, 260)	(246, 252)	16.1	(253, 232)	28.9	(227, 241)	38.1

4. Conclusions

In this paper, an impact localization system of CFRP is proposed. The FBG sensor and narrow-band laser demodulation technology are applied to detect the impact signal of the CFRP structure. The wavelet packet decomposition is introduced to extract different frequency band signals, and the energies of signals are calculated. According to the relationship between the energies and distance from the impact point to FBG sensor, the localization system based on the FBG sensor network and ELM is established for the impact localization. The localization system is verified on the 500 mm × 500 mm × 2 mm CFRP plate. The maximum localization error and the minimum localization error are 30.4 mm and 6.7 mm, respectively. The average localization error is 14.2 mm, and the training time is 0.7 s. Compared with the SVR and BP neural network, the ELM has better results and less training time consumption with only one adjusted parameter. In conclusion, the impact localization system and algorithm, which are proposed in this paper, provide the important means and method for the high accuracy impact detection of the CFRP structure.

Acknowledgement

This research is supported by the National Natural Science Foundation of China under Grant Nos. 61503218 and 61705098; Natural Science Foundation of Shandong Province, China under Grant Nos. ZR2017BF042, ZR2016FM36, and ZR2017BF032; Ph. D. Programs Foundation of Ludong University under Grant No. LA2017006.

References

[1] M. Grujicic, B. Pandurangan, W. C. Bell, C. F. Yen, and B. A. Cheeseman, "Application of a dynamic-mixture shock-wave model to the metal-matrix composite materials," *Materials Science and Engineering: A*, 2011, 528(28): 8187–8197.

[2] A. Katunin, K. Dragan, and M. Dziendzikowski, "Damage identification in aircraft composite

structures: a case study using various non-destructive testing techniques," *Composite Structures*, 2015, 127: 1–9.

[3] F. Otero, S. Oller, S. X. Martinez, and O. Salomon, "Numerical homogenization for composite materials analysis. Comparison with other micro mechanical formulations," *Composite Structures*, 2015, 122: 405–416.

[4] H. Singh, K. K. Namala, and P. Mahajan, "A damage evolution study of E-glass/epoxy composite under low velocity impact," *Composites Part B: Engineering*, 2015, 76: 235–248.

[5] J. K. Zhang and X. Zhang, "An efficient approach for predicting low-velocity impact force and damage in composite laminates," *Composite Structures*, 2015, 130: 85–94.

[6] P. Yang, S. S. Shams, A. Slay, B. Brokate, and R. Elhajjar, "Evaluation of temperature effects on low velocity impact damage in composite sandwich panels with polymeric foam cores," *Composite Structures*, 2015, 129: 213–223.

[7] P. Shrestha, J. H. Kim, Y. Park, and C. G. Kim, "Impact localization on composite structure using FBG sensors and novel impact localization technique based on error outliers," *Composite Structures*, 2016, 142: 263–271.

[8] J. S. Yu, D. K. Liang, X. J. Gong, and X. G. Song, "Impact localization for composite plate based on detrended fluctuation analysis and centroid localization algorithm using FBG sensors," *Optik*, 2018, 167: 25–36.

[9] G. Zhao, S. X. Li, H. X. Hu, Y. C. Zhong, and K. Li, "Impact localization on composite laminates using fiber Bragg grating sensors and a novel technique based on strain amplitude," *Optical Fiber Technology*, 2018, 40: 172–179.

[10] T. Fu, Z. C. Zhang, Y. J. Liu, and J. S. Leng, "Development of an artificial neural network for source localization using a fiber optic acoustic emission sensor array," *Structural Health Monitoring*, 2015, 14(2): 168–177.

[11] K. Zhu, X. P. Qing, and B. Liu, "A two-step impact localization method for composite structures with a parameterized laminate model," *Composite Structures*, 2018, 192: 500–506.

[12] G. Zhao, H. X. Hu, S. X. Li, L. S. Liu, and K. Li, "Localization of impact on composite plates based on integrated wavelet transform and hybrid minimization algorithm," *Composite Structures*, 2017, 176: 234–243.

[13] T. Kundua, H. Nakatani, and N. Takeda, "Acoustic source localization in anisotropic plates," *Ultrasonics*, 2012, 52: 740–746.

[14] F. Ciampa and M. Meo, "A new algorithm for acoustic emission localization and flexural group velocity determination in anisotropic structures," *Composites: Part A*, 2010, 41: 1777–1786.

[15] P. Shrestha, Y. Park, and C. G. Kim, "Low velocity impact localization on composite wing structure using error outlier based algorithm and FBG sensors," *Composites Part B*, 2017, 116: 298–312.

[16] P. Shrestha, J. H. Kim, H. Kwon, and C. G. Kim, "Error outlier with weighted median absolute deviation threshold algorithm and FBG sensor based impact localization on composite wing structure," *Composite Structures*, 2017, 180: 412–419.

[17] S. W. Kim and H. Jang, "Impact localization on a composite plate based on error outliers with Pugh's concept selection," *Composite Structures*, 2018, 200: 449–465.

[18] S. Alajlouni, M. Albakri, and P. Tarazaga, "Impact localization in dispersive waveguides based on energy-attenuation of waves with the traveled distance," *Mechanical Systems & Signal Processing*, 2018, 105: 361–376.

[19] S. Z. Lu, M. S. Jiang, Q. M. Sui, Y. Z. Sai, and L. Jia, "Low velocity impact localization system of CFRP using fiber Bragg grating sensors," *Optical Fiber Technology*, 2015, 21: 13–19.

[20] G. Huang, Q. Zhu, and C. K. Siew, "Extreme learning machine: theory and applications," *Neurocomputing*, 2006, 70(1): 489–501.